

# Measurement of Ferromagnetic resonance in thin films

Aaditya Mishra

*A dissertation submitted for the partial fulfillment of BS-MS dual  
degree in Science*

Under the guidance of  
**Dr. Ananth Venkatesan**



INDIAN INSTITUTE OF SCIENCE EDUCATION AND  
RESEARCH MOHALI

**Aaditya Mishra**

*Measurement of Ferromagnetic resonance in thin films*

MS Thesis, 15 March 2021

Supervisor: **Dr. Ananth Venkatesan**

*Ultra Low Temperature Physics Group*

Department of Physical Sciences

Indian Institute of Science Education and Research Mohali

Knowledge city Sector 81


SAS Nagar Punjab India 140306

## Certificate of Examination


This is to certify that the dissertation titled “**Measurement of Ferromagnetic resonance in thin films**” submitted by **Aaditya Mishra** (Reg. No. MS16131) for the partial fulfillment of BS-MS dual degree programme of the Institute, has been examined by the thesis committee duly appointed by the Institute. The committee finds the work done by the candidate satisfactory and recommends that the report be accepted.



Dr. Kamal P. Singh



Dr. Sudeshna Sinha



Dr. Ananth Venkatesan  
(Supervisor)

Dated: 09/05/2021



## Declaration

The work presented in this dissertation has been carried out by me under the guidance of Dr. Ananth Venkatesan at the Indian Institute of Science Education and Research Mohali.

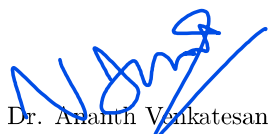
This work has not been submitted in part or in full for a degree, a diploma, or a fellowship to any other university or institute. Whenever contributions of others are involved, every effort is made to indicate this clearly, with due acknowledgement of collaborative research and discussions. This thesis is a bonafide record of original work done by me and all sources listed within have been detailed in the bibliography.

Aaditya Mishra

(Candidate)

Dated: 09/05/2021

In my capacity as the supervisor of the candidate's project work, I certify that the above statements by the candidate are true to the best of my knowledge.



Dr. Ananth Venkatesan  
(Supervisor)



## Acknowledgements

I would like to thank my thesis supervisor Dr. Ananth Venkatesan for providing guidance and support during the project. I also thank my parents for providing moral support. I pay my sincere gratitude to Shelender Sir for mentoring and guiding me during the project. I would like to thank Shyam Sir for helping me during the project. I would also like to thank my friends Abhishek, Akhil, Aman, Aritra, Ojas, Pati, Vivek for their continued support during my stay at IISER Mohali.





# LIST OF FIGURES

Figure 1.1	(a) The magnetization $\mathbf{M}$ precesses with respect to effective magnetic field $\mathbf{H}_{eff}$ according to Landau-Lifshitz equation (b) Change in the precession of magnetization after introducing Gilbert's damping parameter. . . . .	5
Figure 1.2	Common thin film configurations . . . . .	5
Figure 2.1	Schematic of VNA-FMR setup . . . . .	7
Figure 2.2	Representative VNA-FMR data showing the normalized permeability parameter $U$ of a 50 nm thick NiFe film [Kalarickal et al., 2006] . . . . .	8
Figure 2.3	Block diagram of High-sensitivity VNA-FMR measurement apparatus employing microwave interferometer for magnetic nano-dots [Tamaru et al., 2014] . . . . .	9
Figure 2.4	The spectrum showing FMR response of 800 nm diameter and 5 nm thick CoFeB single dot. Solid and dotted lines are plots of real and imaginary parts of $S_{21}$ respectively [Tamaru et al., 2014] . . . . .	10
Figure 2.5	(a) Schematic of Michelson-type interferometer (b) Schematic depiction of scattering processes in the interferometer for $\beta L = n\pi$ [Edwards et al., 2017] . . . . .	11
Figure 2.6	(a) Sample-loaded $S_{11}$ as measured with a two-port VNA as a function of bias magnetic field. (b) Sample-loaded $S_{21}$ as measured with a two-port VNA as a function of bias magnetic field. . . . .	11
Figure 3.1	Microstrip . . . . .	13
Figure 3.2	Two-port incident and reflected wave . . . . .	14
Figure 3.3	Simplified VNA schematic for two-port complex S-parameter measurement . . . . .	15
Figure 3.4	Rohde & Schwarz ZVB 14 VNA . . . . .	15
Figure 3.5	Proposed setup 1 . . . . .	16
Figure 3.6	Microstrip T-junction . . . . .	17
Figure 3.7	Proposed setup 2 . . . . .	17

Figure 4.1	PCBs for setup . . . . .	19
Figure 4.2	Microstrip T-junction with sample . . . . .	19
Figure 4.3	Calibration of electromagnet . . . . .	20
Figure 4.4	Plots of relative $S_{21}$ (a.u.) for different configurations . . . . .	21

# **Abstract**

Ferromagnetic materials have important application in spin electronic devices primarily in developing electronic memories. Measurement of ferromagnetic resonance(FMR) is useful in studying spin properties of ferromagnetic thin films and characterizing magnetic materials. Here we discuss a theoretical model given by Landau, Lifshitz and Gilbert to explain this phenomenon. Further we focus on developing a setup to detect ferromagnetic resonance (FMR) in thin-films using microwave circuits.



# Contents

	Page
ACKNOWLEDGEMENTS	i
LIST OF FIGURES	iii
ABSTRACT	v
<b>1 INTRODUCTION</b>	<b>1</b>
1.1 Interactions in ferromagnets . . . . .	2
1.2 Magnetization dynamics . . . . .	4
<b>2 FMR MEASUREMENT TECHNIQUES</b>	<b>7</b>
2.1 VNA-FMR . . . . .	7
2.2 Interferometric FMR . . . . .	8
2.2.1 High-sensitivity VNA-FMR . . . . .	8
2.2.2 Michelson-type interferometric method . . . . .	10
<b>3 EXPERIMENTAL SETUP</b>	<b>13</b>
3.1 Basics of microwave circuits . . . . .	13
3.1.1 Microstrip . . . . .	13
3.1.2 S-parameters . . . . .	14
3.1.3 Vector Network Analyzer . . . . .	15
3.2 Setup . . . . .	16
3.2.1 Proposed setup 1 . . . . .	16
3.2.2 Proposed setup 2 . . . . .	16
<b>4 PROGRESS</b>	<b>19</b>
4.1 PCB design and production . . . . .	19

4.2	Application of external magnetic field . . . . .	20
4.3	S-parameter measurement . . . . .	20

BIBLIOGRAPHY		<b>23</b>
--------------	--	-----------

## Chapter 1

# INTRODUCTION

---

Spintronics is a field of research that aims to use the spin degree of freedom of electrons to create new electronic devices, especially in the memory domain. The intrinsic angular momentum of a particle, which produces a magnetic dipole moment, is defined from spin. Without an external magnetic field to align the spins, there is no large-scale spin order in most materials. In ferromagnetic and ferrimagnetic materials, however, due to the presence of an exchange interaction which aligns neighbouring spins, a spontaneous magnetic order occurs even in the absence of an applied magnetic field.

Since the switching current of a spintronic magnetic memory cell is proportional to the damping of the spin dynamics of the magnetic material, a small magnetization damping is preferred for fast writing and reading speeds as well as low energy consumption. As a result, a thorough understanding of the dynamic response of small magnetic elements to high frequency magnetic fields will be required to push device performance closer to fundamental limits. Ferromagnetic resonance (FMR) is an important technique for measuring the bulk spin properties of ferromagnetic materials and thin films, and the primary focus of this report is the development of techniques for measuring FMR and characterising a multifaceted experimental FMR setup.

The mutual excitation of an ensemble of electron spin magnetic moments in a magnetic solid is known as ferromagnetic resonance (FMR). During experiment, the sample is exposed to a fixed frequency microwave field as well as a static field. The reflected or absorbed power from the solution is recorded at each field value. This can produce one

or more minima and maxima, corresponding to ensemble resonance modes. The resonance field, also known as the resonance field, is determined by a collection of magnetic parameters. Since magnetic moments in ferromagnets experience not only the applied field, but also dipole-dipole coupling between moments, direct exchange interactions, and spin-orbit interactions. Demagnetizing forces, exchange fields in the case of non-uniform magnetic moment orientations, magneto-crystalline anisotropy torques, magneto-elastic torques, and dissipative torques are all generated as a result of these processes. Torque or effective field can also be contributed by a magnetic interlayer coupling. Since the overall effective field, and hence the resonance field, is dependent on these conditions, FMR is a valuable method for determining the related magnetic parameters.

## 1.1 Interactions in ferromagnets

In ferromagnets, the domain structure is produced by the combination of several interactions. In order to explain the dynamics, it's also necessary to understand the energy landscape formed by these interactions. The magnetization ( $\mathbf{M}$ ) is given by the magnetic moment per unit volume.[Alex Hubert, 1998]

- **Exchange interaction:** The exchange interaction is based on the Coulomb interaction in conjunction with the Pauli exclusion rule, which states that two fermions cannot be in the same quantum state. In solids, total energy due to spins ( $\mathbf{S}$ ) of  $N$  atoms is given by the Heisenberg model,

$$E_{ex} = - \sum_{i,j}^N J_{ij} \mathbf{S}_i \mathbf{S}_j = -2 \sum_{i < j}^N J_{ij} \mathbf{S}_i \mathbf{S}_j \quad (1.1)$$

where  $J_{ij}$  is exchange integral. For ferromagnetic materials, energy is lower in parallel alignment of spins due to positive sign of  $J_{ij}$ . In mesoscopic-level, the exchange energy density is given by,

$$\varepsilon_{ex} = \frac{nJS^2}{aV} \int dV (\nabla \mathbf{m}) \quad (1.2)$$

where  $\mathbf{m} = \mathbf{M}/M_s$  is normalized magnetization,  $M_s$  being the saturation magnetization,  $a$  is the lattice constant and  $n$  is a factor dependent on crystal structure.

- **Zeeman interaction:** The energy resulting from interaction of the magnetization



( $\mathbf{M}$ ) with the external magnetic field ( $\mathbf{H}_{ext}$ ) is given by,

$$\varepsilon_{zee} = \frac{-\mu_0}{V} \int dV \mathbf{M} \cdot \mathbf{H}_{ext} \quad (1.3)$$

- **Anisotropic interactions:** The energy of a magnetic sample is generally determined by the direction of magnetization. The spin-orbit coupling explains shape anisotropy: the spins are bound to the orbital angular momentum, whose energy is linked to its orientation relative to the crystal lattice. For solids having cubic lattice structure, magnetocrystalline anisotropic energy density is given by

$$\varepsilon_{ani} = K_1(m_x^2 m_y^2 + m_y^2 m_z^2 + m_x^2 m_z^2) + K_2 m_x^2 m_y^2 m_z^2 \quad (1.4)$$

here  $m_i$  are the components of normalized magnetization  $\mathbf{m}$  and  $K_1, K_2$  are the anisotropy constant of first and second order. Energy density due to uniaxial magnetocrystalline anisotropy is given by

$$\varepsilon_{uni} = -K_u m_x^2 \quad (1.5)$$

here  $K_u$  is the uniaxial anisotropy constant describing the preferred axis of magnetization in the material. In thin films, apart from volume anisotropies, surface anisotropy is also significant. It is described using perpendicular anisotropy constant ( $K_\perp$ )

$$\varepsilon_{sur} = -\frac{K_\perp}{d} m_z^2 \quad (1.6)$$

- **Demagnetization field interaction:** The dipolar interaction between magnetic moments has a very long range. Each magnetic moment interacts with the dipolar field of every other magnetic moment, resulting in a non-local demagnetizing energy contribution.

$$\varepsilon_{dem} = \frac{-\mu_0}{2V} \int dV \mathbf{M} \cdot \mathbf{H}_{dem} \quad (1.7)$$

For uniformly magnetized ellipsoid, demagnetizing field is given by

$$\mathbf{H}_{dem} = -\mathbf{N} \cdot \mathbf{M} \quad (1.8)$$

where  $\mathbf{N}$  is demagnetizing matrix given by

$$\mathbf{N} = \begin{bmatrix} N_x & 0 & 0 \\ 0 & N_y & 0 \\ 0 & 0 & N_z \end{bmatrix} \quad (1.9)$$

here,  $(N_x, N_y, N_z)$  are demagnetizing factors. The equation (1.7) can also be rewritten in a simpler form,

$$\varepsilon_{dem} = \frac{\mu_0}{2} \mathbf{M} \cdot \mathbf{N} \cdot \mathbf{M} \quad (1.10)$$

## 1.2 Magnetization dynamics

The effective magnetic field on thin-film can be calculated by taking functional derivative of total energy density due to various interactions with respect to magnetization

$$\mathbf{H}_{eff} = -\frac{1}{\mu_0} \nabla_{\mathbf{M}} (\varepsilon_{ex} + \varepsilon_{zee} + \varepsilon_{ani} + \varepsilon_{uni} + \varepsilon_{sur} + \varepsilon_{dem}) \quad (1.11)$$

Landau and Lifshitz(LL) introduced a model in 1935 describing the precession of magnetization  $\mathbf{M}$  vector in presence of effective magnetic field  $\mathbf{H}_{eff}$ :

$$\frac{d\mathbf{M}}{dt} = -\gamma\mu_0 \mathbf{M} \times \mathbf{H}_{eff} \quad (1.12)$$

where  $\gamma = g \frac{|e|\hbar}{2m_e}$  is the gyromagnetic ratio,  $g$  is the Landé g-factor,  $e$  is the electronic charge and  $m_e$  is the mass of electron.

The LL equation predicts undamped precession of  $\mathbf{M}$  around  $\mathbf{H}_{eff}$  at a constant cone angle. However, it was observed experimentally that magnetization aligns with  $\mathbf{H}_{eff}$  after a finite time. To account for this inconsistency, Gilbert in 1955 proposed adding a damping term to the LL equation. The Landau-Lifshitz-Gilbert(LLG) equation is given by,

$$\frac{d\mathbf{M}}{dt} = -\gamma\mu_0 \mathbf{M} \times \mathbf{H}_{eff} + \frac{\alpha}{M_s} \left( \mathbf{M} \times \frac{d\mathbf{M}}{dt} \right) \quad (1.13)$$

The LLG equation can also be equivalently written in a form similar to LL equation.

$$\frac{d\mathbf{M}}{dt} = -\frac{\gamma\mu_0}{(1+\alpha^2)} \mathbf{M} \times \mathbf{H}_{eff} - \frac{\gamma\mu_0\alpha}{M_s(1+\alpha^2)} \mathbf{M} \times (\mathbf{M} \times \mathbf{H}_{eff}) \quad (1.14)$$

The final solution for the precession frequency is given by Kittel's equation,

$$\omega_{res}^2 = \gamma^2 \mu_0^2 (H_{ext} + H_{uni} + (N_z - N_x)M_s)(H_{ext} + H_{uni} + (N_y - N_x)M_s) \quad (1.15)$$

For two common orientation of film, in-plane field(i.e.  $N_x = 1, N_y, N_z = 0$ ),

$$\omega_{res} = \gamma\mu_0 (H_{ext} + H_{uni} - M_s) \quad (1.16)$$

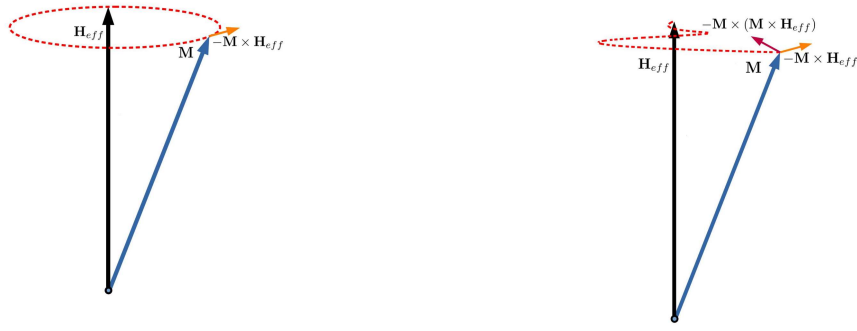


Figure 1.1: (a) The magnetization  $\mathbf{M}$  precesses with respect to effective magnetic field  $\mathbf{H}_{eff}$  according to Landau-Lifshitz equation (b) Change in the precession of magnetization after introducing Gilbert's damping parameter.

and for out of plane field(i.e.  $N_x, N_y = 0, N_z = 1$ ),

$$\omega_{res} = \gamma\mu_0 \sqrt{(H_{ext} + H_{uni})(H_{ext} + H_{uni} + M_s)} \quad (1.17)$$



Figure 1.2: Common thin film configurations

To compensate for damping loss, an AC magnetic field perpendicular to the static bias field may be applied to drive the magnetization precession. At resonance, the microwave frequency matches the magnetization precession frequency, and maximal power is transmitted from the microwave to the sample. This is FMR condition, and the combined activity of the sample can be determined by analysing the microwave power absorption profile.



## Chapter 2

# FMR MEASUREMENT TECHNIQUES

---

### 2.1 VNA-FMR

One of the broadband FMR measurement method having high signal to noise ratio is VNA-FMR . In this setup, vector network analyzer is connected to co-planar wave guide (CPW) of impedance  $50\Omega$  which is used to excite the ferromagnetic sample. The sample is placed over the CPW with the magnetic film facing the CPW.

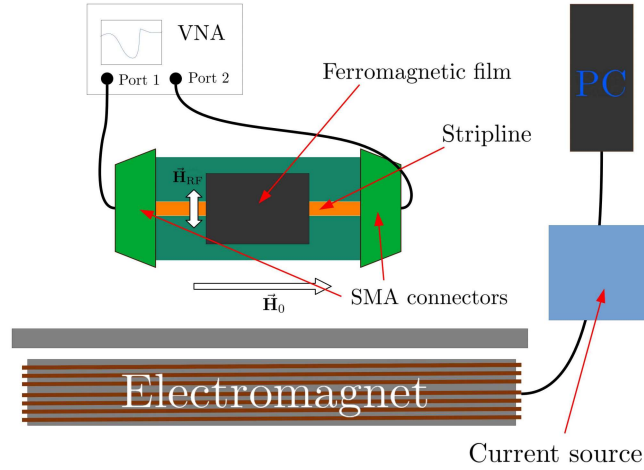


Figure 2.1: Schematic of VNA-FMR setup

[Kalarickal et al., 2006] analyzed the data using effective microwave permeability parameter of the form

$$U(f) = \pm i \frac{\ln(S_{21-H}(f)) - \ln(S_{21-ref}(f))}{\ln(S_{21-ref}(f))} \quad (2.1)$$

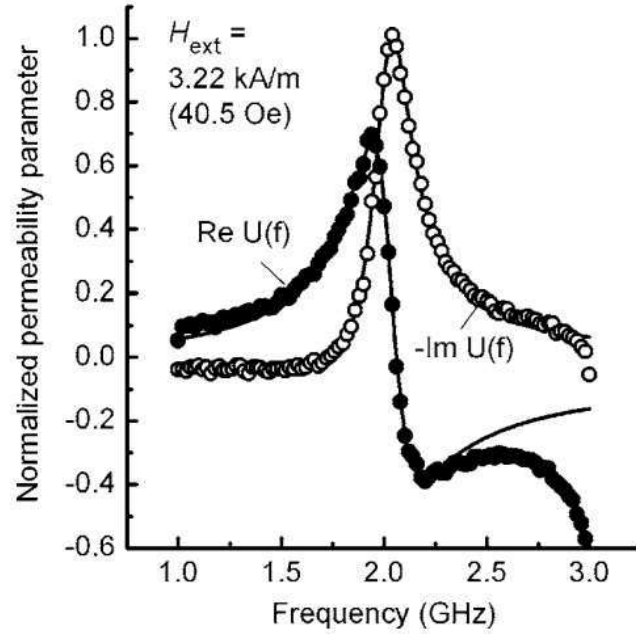


Figure 2.2: Representative VNA-FMR data showing the normalized permeability parameter  $U$  of a 50 nm thick NiFe film [Kalarickal et al., 2006]

here,  $f$  denotes the frequency of measurement,  $S_{21-H}$  and  $S_{21-ref}$  are respectively the scattering parameters  $S_{21}$  at a given value of static external magnetic field of interest and at a reference field.

## 2.2 Interferometric FMR

### 2.2.1 High-sensitivity VNA-FMR

Here, the sensitivity of the FMR measurement is increased by combining the high sensitivity of the VNA-FMR measurement, and the improvement in signal-to-noise ratio of a microwave interferometer via background subtraction. Figure 2.3 shows the block diagram of the apparatus. Here, abbreviations of components are as follows, PR are probes, PD is power divider, PS is phase shifter, VA is variable attenuator, LNA is low-noise amplifier, EM is electromagnet, CS is current source for EM, SG is signal generator and AWG is arbitrary waveform generator. The signal is split in two parts, one is passed through CPW

exciting the ferromagnetic sample and other part passes through phase shifter and variable attenuator. Phase shifter and variable attenuator are adjusted such that when there is no FMR, signal is of the same amplitude as path 1 and has a phase difference of  $180^\circ$ . Ideally, without any FMR, there is no signal after PC since signals from path 1 and 2 interfere destructively forming a Mach-Zehnder type interferometer.

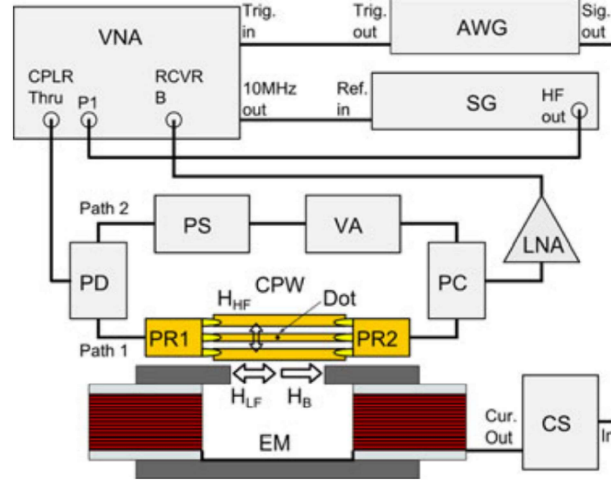


Figure 2.3: Block diagram of High-sensitivity VNA-FMR measurement apparatus employing microwave interferometer for magnetic nano-dots [Tamaru et al., 2014]

In FMR condition, due to absorption by ferromagnetic sample, signal in path 1 acquires phase shift and amplitude modulation thus violating the destructive interferometric condition. The difference is further amplified by LNA and recorded using VNA. This method provides significant improvement in SNR since background signals destructively interfere and get cancelled.

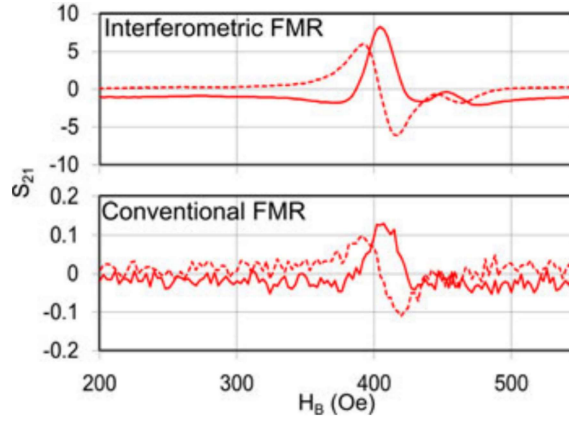


Figure 2.4: The spectrum showing FMR response of 800 nm diameter and 5 nm thick CoFeB single dot. Solid and dotted lines are plots of real and imaginary parts of  $S_{21}$  respectively [Tamaru et al., 2014]

### 2.2.2 Michelson-type interferometric method

This setup uses CPW in cross junction with two short-terminal arms of equal length (Figure 2.5(a)). This cross junction forms a Michelson-type microwave interferometer which at discrete frequencies (determined by arm length  $L$ ), allows for high sensitivity magnetic field-sweep measurements as background gets suppressed. Frequencies at which destructive interference occurs is calculated by solving  $\beta L = n\pi$  condition, here,  $\beta = 2\pi n_{eff}f/c$  is the transmission line phase constant,  $f$  is the frequency and  $c$  is speed of light. At these frequencies, there is constructive interference at port 1 and destructive at port 2. Sample is placed on one of the shorted arms of the interferometer which under FMR condition absorbs and phase shifts the signal and breaks the interferometric relation.



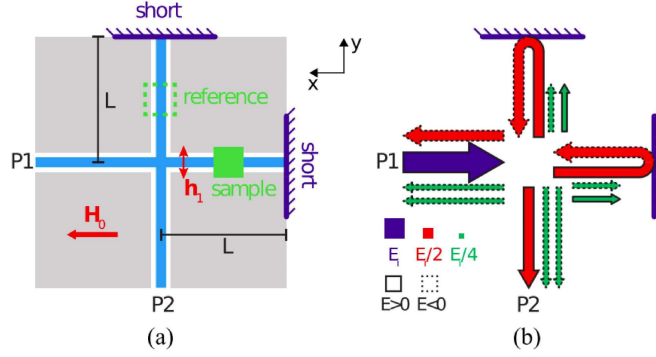


Figure 2.5: (a) Schematic of Michelson-type interferometer (b) Schematic depiction of scattering processes in the interferometer for  $\beta L = n\pi$  [Edwards et al., 2017]

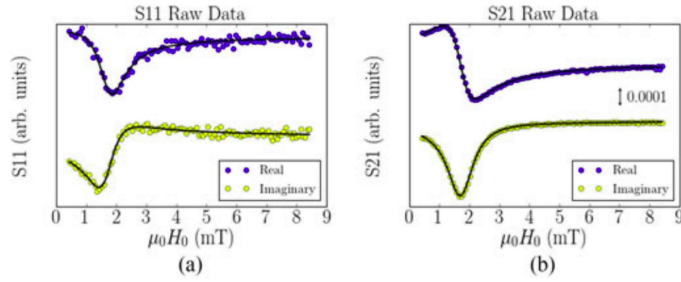


Figure 2.6: (a) Sample-loaded S11 as measured with a two-port VNA as a function of bias magnetic field. (b) Sample-loaded S21 as measured with a two-port VNA as a function of bias magnetic field.



## Chapter 3

# EXPERIMENTAL SETUP

---

### 3.1 Basics of microwave circuits

#### 3.1.1 Microstrip

One of the most common types of planar transmission lines is the microstrip line, which can be manufactured using photolithographic processes. Microstrip propagates quasi TM-TE

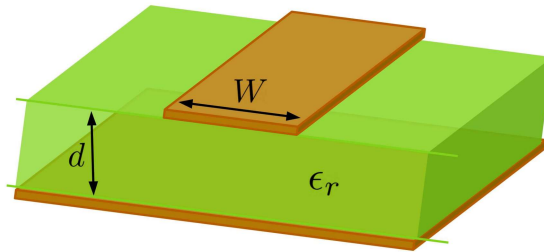


Figure 3.1: Microstrip

mode which is utilized to apply excitation rf magnetic wave.

Characteristic impedance of microstrip of given conductor width  $W$ , substrate thickness  $d$  and relative permittivity  $\epsilon_r$  can be calculated for  $W/d > 1$  using

$$Z_0 = \frac{120\pi}{\sqrt{\epsilon_r}(W/d + 1.393 + 0.667 \ln(W/d + 1.444))} \quad (3.1)$$

where  $\epsilon_e$  is effective dielectric constant of the microstrip given by,

$$\epsilon_e = \frac{\epsilon_r + 1}{2} + \frac{\epsilon_r - 1}{2} \left( \frac{1}{\sqrt{1 + 12d/W}} \right) \quad (3.2)$$

In order to reduce power loss reflections from ports connecting to measurement devices, it is important to match the characteristic impedance of transmission line to that of the ports(i.e.  $Z_0 = 50\Omega$ ). Microstrip was made using FR4-epoxy as a substrate having relative permittivity  $\epsilon_r = 4.4$  and thickness  $d = 1.6mm$ . Width of central conductor ( $W = 3mm$ ) is calculated by substituting  $Z_0$ ,  $d$  and  $\epsilon_e$  in equation (3.1).

### 3.1.2 S-parameters

Voltages and currents cannot be defined uniquely in waveguides that support non-TEM propagation. It is desirable for these systems to incorporate scattering parameters, also known as S-parameters, which correlate incident and reflected electromagnetic waves. S-parameters help one to avoid absolute voltage and current measurements, which become complicated at high frequencies. The complex wave amplitudes  $a_i, b_i$  at port  $i$  is given for of voltage  $V_i$ , current  $I_i$  and impedance  $Z_{ci}$  as

$$a_i = \frac{V_i + Z_{ci}I_i}{2\sqrt{Z_{ci}}} \quad ; \quad b_i = \frac{V_i - Z_{ci}I_i}{2\sqrt{Z_{ci}}} \quad (3.3)$$

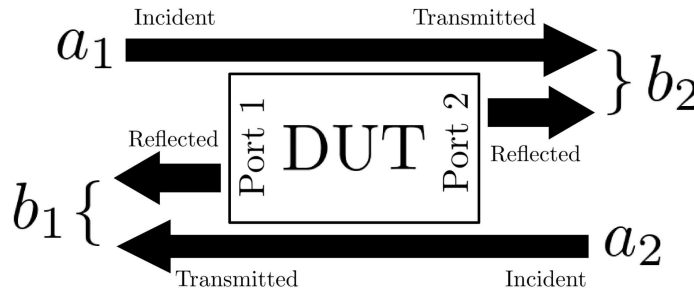


Figure 3.2: Two-port incident and reflected wave

For two-port measurements, the relationship between  $a_{1,2}$  and  $b_{1,2}$  is given by

$$\begin{bmatrix} b_1 \\ b_2 \end{bmatrix} = \begin{bmatrix} S_{11} & S_{12} \\ S_{21} & S_{22} \end{bmatrix} \begin{bmatrix} a_1 \\ a_2 \end{bmatrix} \quad \text{where} \quad S_{ij} = \frac{b_j}{a_i} \quad (3.4)$$

### 3.1.3 Vector Network Analyzer

Vector network analyzer(VNA) is used to measure complex S-parameters of the DUT. A synthesized high-frequency source in VNA provides signal at measurement frequency  $f$ .

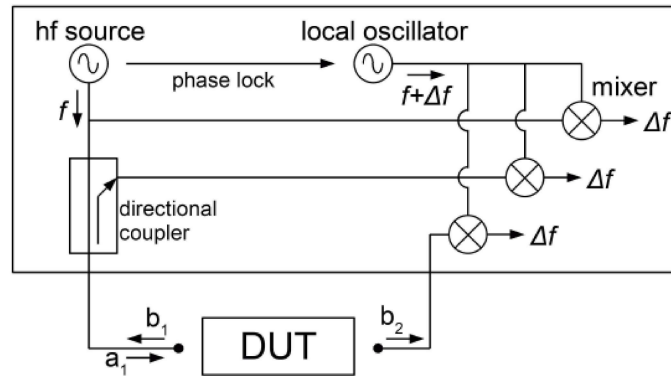


Figure 3.3: Simplified VNA schematic for two-port complex S-parameter measurement

We used Rohde & Schwarz ZVB 14 VNA, which measures phase sensitive complex S-parameter in frequency range of  $10MHz$  to  $14GHz$ .

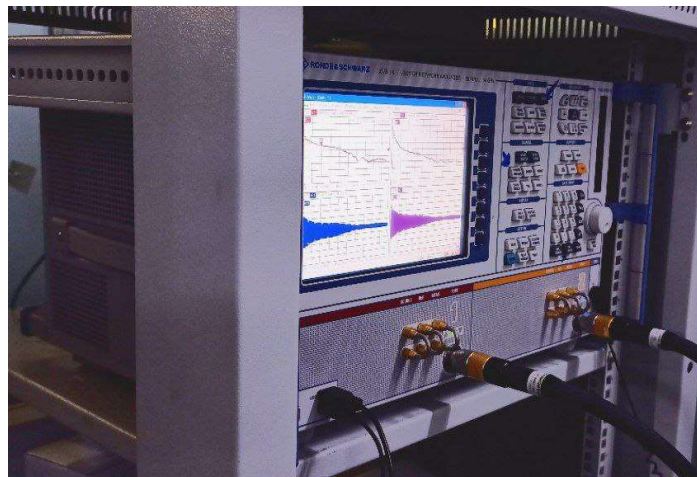


Figure 3.4: Rohde & Schwarz ZVB 14 VNA

## 3.2 Setup

Permalloy sample thin film having 40nm thickness was produced using thermal evaporator. Film was then placed on microstrip in flip-chip configuration using vacuum grease. We have used two designs of microstrip for FMR measurement.

### 3.2.1 Proposed setup 1

In this setup, sample is placed on a two port microstrip transmission line of which scattering parameters is measured using VNA. External magnetic field is applied using electromagnet and film configuration is adjusted by placing the microstrip perpendicular and parallel to the magnetic field. SMA connectors are used to connect the ports of microstrip to coaxial cable which is then connected to ports of VNA. A schematic representing this setup is shown in Figure 3.5.

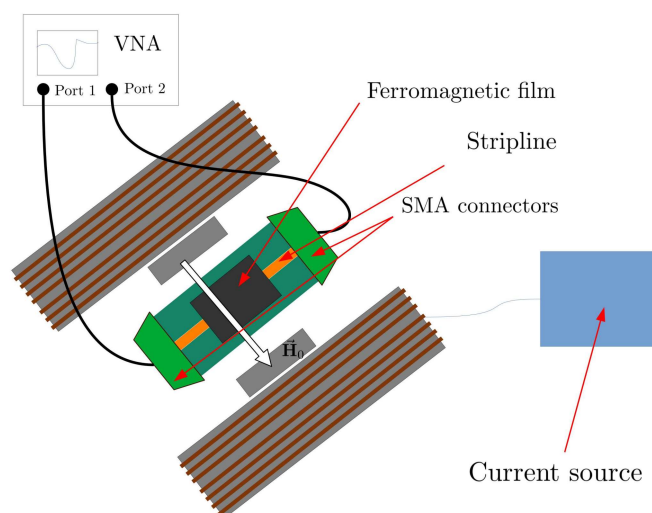


Figure 3.5: Proposed setup 1

### 3.2.2 Proposed setup 2

This setup consists of 3-port microstrip T-junction (Figure 3.6). Two ports of the T-junction are connected to 3dB power splitter having  $180^\circ$  phase difference between them and the third port is used for output signal. Without any FMR output from third port should be close

to zero since the input signals cancel each other. When in FMR condition, input signals fail to cancel out due to absorption of signal by the film. This setup shares analogy with Michelson interferometer and promises improvements in FMR detection. Figure 3.7 shows representation of this setup.



Figure 3.6: Microstrip T-junction

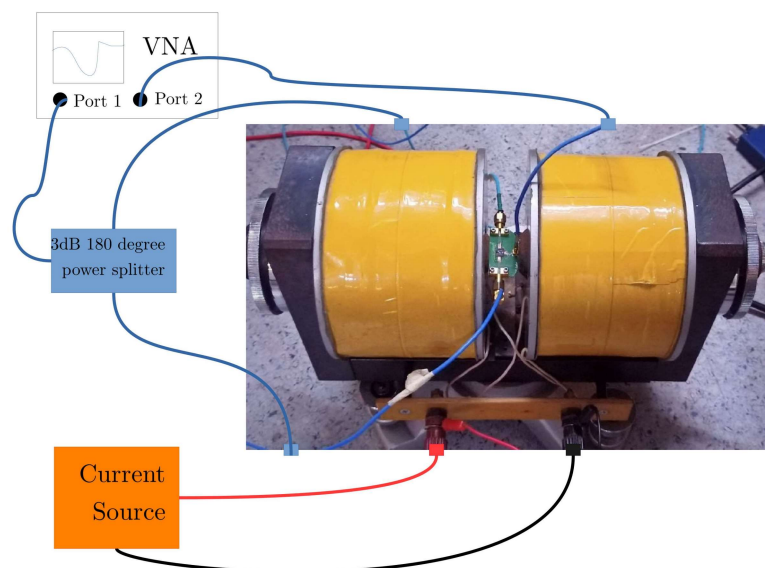


Figure 3.7: Proposed setup 2





## Chapter 4

# PROGRESS

---

### 4.1 PCB design and production

Microstrips are designed using KiCAD with width  $W = 3mm$ , calculated in 3.1.

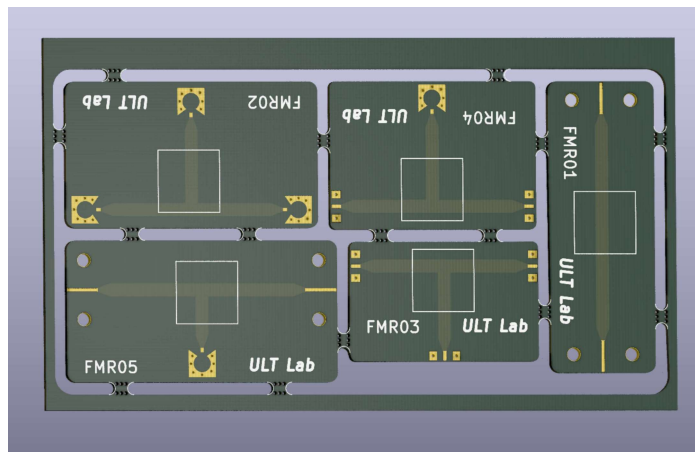


Figure 4.1: PCBs for setup

Figure 4.2 shows a microstrip with sample attached.

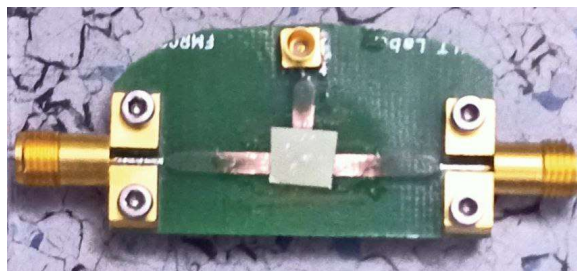


Figure 4.2: Microstrip T-junction with sample

PCBs were manufactured using FR4-epoxy as substrate of thickness  $d = 1.6\text{mm}$ .

## 4.2 Application of external magnetic field

For measuring the magnetic field near the sample, gauss probe was used to calibrate magnetic field produced by electromagnet with the applied current and the result is shown in Figure 4.3. Excitation magnetic field of small magnitude is applied by passing AC through microstrip on which ferromagnetic sample is placed.

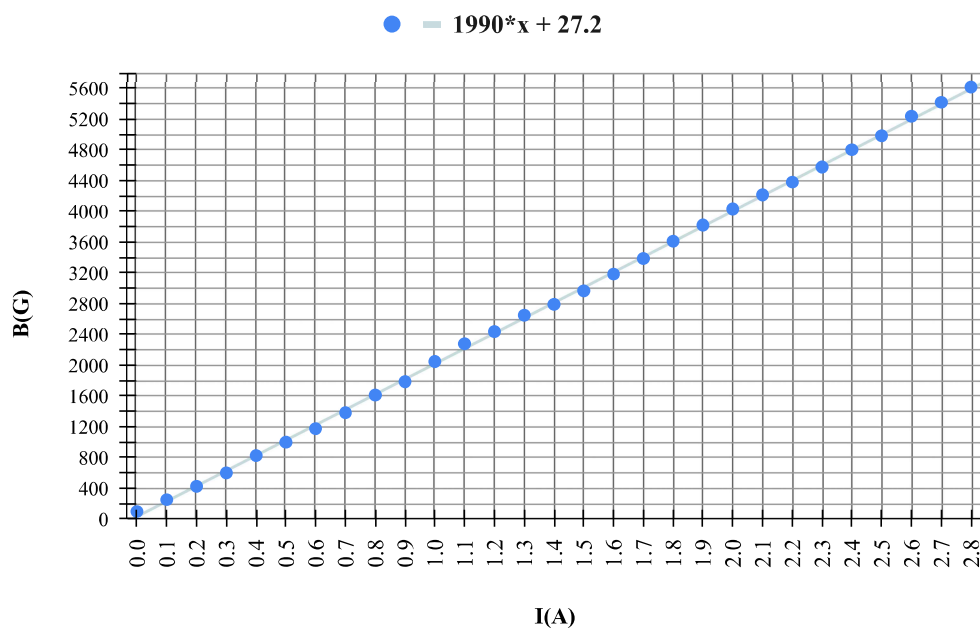
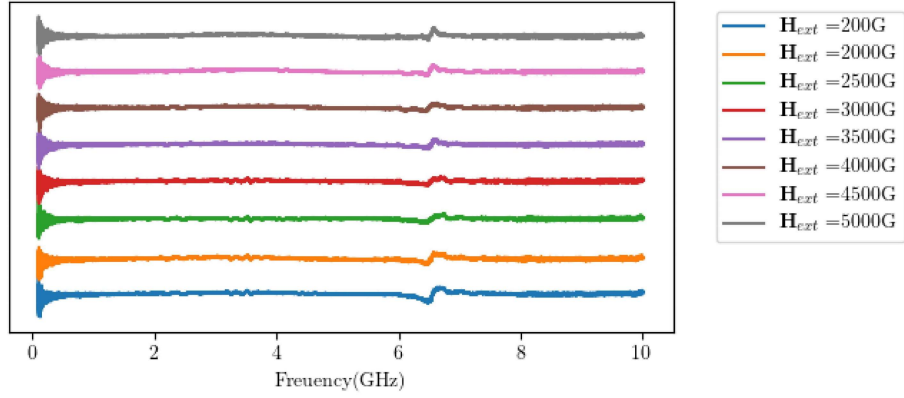


Figure 4.3: Calibration of electromagnet

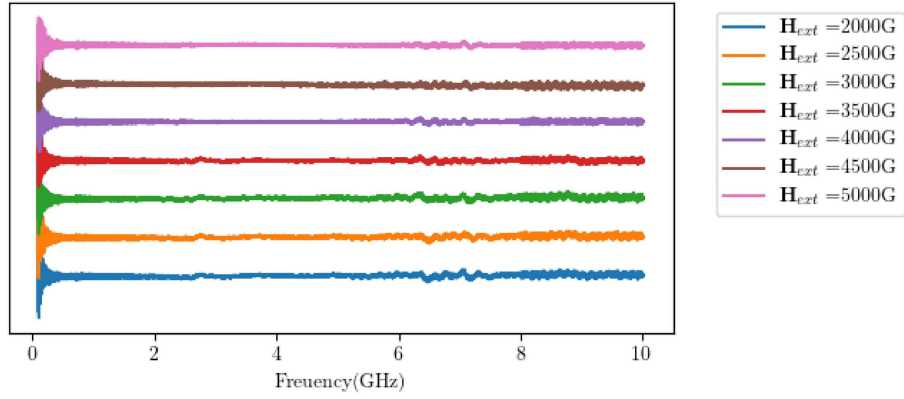
## 4.3 S-parameter measurement

We have measured scattering parameters for proposed setup 1 in in-plane and perpendicular configuration and for proposed setup 2 in in-plane configuration. Thus far, we have not detected the FMR absorption in the sample and further measurements and data analysis is required.  $S_{21}$  is recorded for external magnetic fields ranging from 200G to 5500G. Relative  $S_{21}$  is calculated by subtracting background from that of  $S_{21}$  at different magnetic fields.

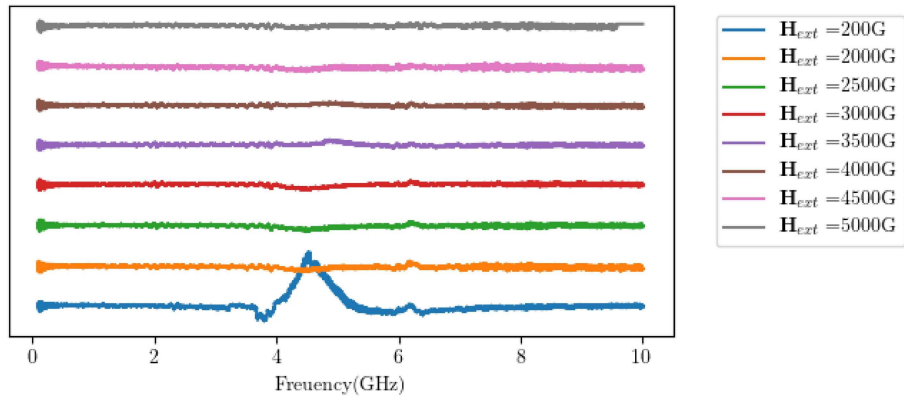
Figure 4.4: Plots of relative  $S_{21}$ (a.u.) for different configurations



(a) In-plane configuration, proposed setup 1



(b) perpendicular configuration, proposed setup 1



(c) In-plane configuration, proposed setup 2



# BIBLIOGRAPHY

---

- [Alex Hubert, 1998] Alex Hubert, R. S. (1998). *Magnetic Domains*. Springer-Verlag Berlin Heidelberg.
- [Edwards et al., 2017] Edwards, E. R. J., Kos, A. B., Weiler, M., and Silva, T. J. (2017). A microwave interferometer of the michelson-type to improve the dynamic range of broadband ferromagnetic resonance measurements. *IEEE Magnetics Letters*, 8:1–4.
- [Kalarickal et al., 2006] Kalarickal, S. S., Krivosik, P., Wu, M., Patton, C. E., Schneider, M. L., Kabos, P., Silva, T. J., and Nibarger, J. P. (2006). Ferromagnetic resonance linewidth in metallic thin films: Comparison of measurement methods. *Journal of Applied Physics*, 99(9):093909.
- [Tamaru et al., 2014] Tamaru, S., Yakushiji, K., Fukushima, A., Yuasa, S., and Kubota, H. (2014). Ultrahigh sensitivity ferromagnetic resonance measurement based on microwave interferometer. *IEEE Magnetics Letters*, 5:1–4.